Light refraction in the Earth's atmosphere III. Inferior mirages: images locus

C. Alejandro Paola[a,b], A. Cruzado[a,c], and A. Cesanelli[a]

[a]*Facultad de Ciencias Astronómicas y Geofísicas, Univesidad Nacional de La Plata, Paseo del Bosque s/n, La Plata, Buenos Aires, Argentina; TE: (54) 221 4236593. Fax: (54) 221 4236591. e-mail: apaola@fcaglp.unlp.edu.ar; acesanelli@fcaglp.unlp.edu.ar*

[b]*Universidad Tecnológica Nacional, Facultad Regional La Plata, Avenida 60 esquina 124 s/n, La Plata, Buenos Aires, Argentina; Tel: (54) 221 4124300.*

[c]*Instituto de Astrofísica de La Plata, Paseo del Bosque s/n, 1900 La Plata, Buenos Aires, Argentina e-mail: acruzado@fcaglp.unlp.edu.ar; alicehaiadjamian@yahoo.com.ar*

Received 30 August 2023; accepted 6 November 2023

Our main goal is to find the locus of images formed as a result of an inferior mirage. To achieve our goal we first show that provided the beam entering a detection system has a small aperture, the image of a point object formed by that system in a vertical plane passing through the object is a point. This holds regardless of whether the image formed by an optical system previously traversed by the beam has generated a non-point image of the object. Secondly, we show that the different images formed by the detection system, as its position relative to the object varies, are located on the caustic curve corresponding to the previously traversed optical system. Next, we derive the analytical expressions for the caustic curves corresponding to two particular cases, one of them being the inferior mirages. These expressions have been obtained through of the Legendre antitransform of the asymptotic lines to the paths of light rays reaching the detector. For the case of inferior mirages, we have studied in detail the locus of the images in each vertical plane passing through the object as a function of the position of the object relative to the ground, its position relative to the detector, and the atmospheric conditions. Finally, we get somewhat into the matter of the image's position as it would be seen by a casual observer of an inferior mirage.

Keywords: Planetary atmospheres; light refraction; inferior mirages; analytic expression.

DOI: https://doi.org/10.31349/RevMexFis.70.031301

1. Introduction

This is one of a series of works in which we intend to deal with different optical phenomena taking place in planetary atmospheres. We have begun the series by addressing the study of one of the countless phenomena related to light refraction in the Earth's atmosphere: inferior mirages. In the first work of this series [13] we have dealt with the heat transport through the microlayer to obtain the refractive index profile in air and, from it and applying Fermat's extremal principle, we found an analytical expression that describes the path of light rays through the atmosphere. In a second work, we have addressed our attention to the search for viewing regions of inferior mirages in a plane perpendicular to the ground depending on the position of the observer and the atmospheric conditions (Cruzado *et al*., 2023 [8]). Our objective was then to know if, given the horizontal distance to the object, d_{ob}, and the height from the ground, y_{ob}, under specific atmospheric conditions, an observer would be able to visualize the object and/or its image, or none of them.

In the present work, we are interested in the locus of the images on the occasion of inferior mirages. That is, for a given observer position (d_{ob},y_{ob}), within a region from where he/she could see the image of the object, as analyzed in Cruzado *et al*. [8], we look for the pair (x_i,y_i), where x_i and y_i are the horizontal distance to the object and the height from the ground, respectively, at which the image seen by that observer is formed. Our main objective is, ultimately, to find an expression that represents y_i as a function of x_i.

It is well known that most of the refractive phenomena caused by light coming from an isotropic emitter point generate images that, if the solid angle subtended by the beam of rays coming from the source is not small enough, are not points. Then, although the rays of light do not all intersect at the same point, provided azimuthal symmetry with respect to an axis passing through the object exists, a solid of revolution contains all those rays that, coming from the point object, have passed through the refractive system. Each of these rays is tangent at some point to the boundary surface of that solid, whose projection on a plane is a curve called caustic. Many authors analyze the equation of the caustic curve generated by an optical system, whether refractive or reflective, affected by different types of aberrations. These aberrations typically occur when we move away from the paraxial approximation. In the articles by Lock and Woodruff [12], Da Costa and Escalona [9], Bellver-Cebreros *et al*. [2], Cordero-Dávila and Castro-Ramos [7], Korneĭchik [11], Silva-Ortigoza [14], and Carpena and Coronado [6] the caustics generated in the context of different optical phenomena are analyzed within the

framework of different theories.

Closely related to what we have just said in the previous paragraph is the particular situation that we are interested on, in which the observed images of a point object are points, although their position depend on the observer position. To clarify this point we consider any optical system, refractive or reflective, traversed by a non-paraxial beam of light coming from a point object. After passing through the system, the rays of light, far from all intersecting at the same point, are contained in the solid of revolution limited by the caustic surface corresponding to the particular optical system, provided that azimuthal symmetry exists. All the rays contained in the solid contribute to the formation of the image of the object on a screen placed perpendicular to the optical axis of the system. The image of the point object would then be a spot of light rather than a point, the size of which depends on where the screen is placed. A screen placed where the circle of least confusion is located pick up the sharpest image, being enlarged the size of the luminous spot for smaller or greater distances from the object. However, if instead of placing a screen to collect the image, we place another refractive system with a very small aperture, a small portion of the rays contained in the solid will contribute to the formation of the image by this system. Thus, the image of the point object generated by the second system will be a point. Furthermore, taking into account that rays contributing to the formation of this point image are all tangent to the caustic, then the point image will be, approximately a point of the caustic. The specific point on the caustic curve depends on the position of the second refractive system, since the small beam of rays determines the configuration of the formed image.

This is precisely what happens in each vertical plane passing through the object (hereafter referred as propagation plane) on the occasion of sighting an inferior mirage, when the refractive optical system that collects the image is the human eye. In this case, the beam of light that, after passing through a portion of the atmosphere, enters the observer's eye with a very small aperture. Consequently, the image of a point object formed on the retina is a point. In this article we show that the image position as a function of the observer position is, in each propagation plane, a curve that represents the Legendre antitransform of the asymptotics lines to the rays that reach the observer eye. It is well known that the Legendre antitransform of the lines containing the light rays can be used to determine the caustic equation associated with an optical system. This is because the caustic surface generated by an optical system is precisely the surface to which the light rays, originating from the object, are tangent after passing through the system. So, as long as the equation describing the paths of light rays is known, the Legendre transformations can be used to find the corresponding caustics. They have been used, for example, by Bellver-Cebreros and Rodriguez-Danta [1] to obtain the caustics of light rays reflected in a surface profile, and by Gitin [10] to obtain the caustics of light rays from the transverse aberration of the optical system.

Regarding the topic we are interesting on, the inferior mirages, it can be said that the curve that represents the image position of a point object as a function of the observer position in each vertical plane containing the axis that passes through the object, is nothing more that the caustic curve of the refractive system represented by the atmosphere. Although we are mainly interested on inferior mirages, we will see that the technique developed in this work allows to determine the point image position (x_i, y_i) of a point source as a function of the distance to the object to the optical system that forms the image, whenever the beam of rays entering this system has a small aperture.

We organize the article in the following way: in Sec. 2, we explain the methodology used to show that the curve containing the positions of the images in each vertical plane containing the axis that passes through the object is the Legendre antitransform of the asymptotic lines to the rays reaching any small aperture detector; in Sec. 3, we apply the result found to an elementary case; in Sec. 4, we apply the result found to the inferior mirages; in Sec. 5, we show our results; finally, in Sec. 6, we expose our conclusions.

2. Methodology

First of all, we set that, in analyzing images formation by a physical system, we assume azimuthal symmetry respect to an axis passing through the object. Then, the results obtained in this and the following sections are valid in every plane containing the symmetry axis of the system. Azimuthal symmetry is approximately true in the two situations we consider in the present paper, and the planes containing the axis of symmetry of the system are, in both cases, vertical planes. Then, whenever we refer to the observer eyes, we are actually considering a vertical opening of the light beam equal to the human pupil diameter, but a negligible horizontal opening. Then, what is observed in these propagation planes is, in fact, what would be observed if the optical system that forms the image is a short vertical slit. In Sec. 5, we further discuss what an observer actually sees when exposed to a beam that, in addition to having a vertical aperture of about 3 mm, has a similar horizontal aperture, if viewed the phenomenon with only one eye, or of about 6 cm if viewed with both eyes.

Having established that, let us consider a beam of rays coming from a point object and reaching the pupil of a distant observer. Since in this case the beam of light reaching the observer eye subtends an extremely small solid angle, two rays belonging to the beam have very close slopes, so that the straight lines that contain them can be written as:

$$\begin{cases} y = ux + v\,[u] \\ y = (u + \Delta u)\,x + v\,[u + \Delta u] \end{cases}, \tag{1}$$

where u and $u + \Delta u$ are the slopes of each line, and v (which is a function of u) is the corresponding y-intercept of the line. Since the two lines belong to the same ray beam, they must

intersect each other at the point image with coordinates (x_i,y_i). Solving the previous two equations system we find:

$$x_i = -\frac{v\,[u+\Delta u]-v\,[u]}{\Delta u}, \tag{2}$$

and

$$y_i = -u\frac{v\,[u+\Delta u]-v\,[u]}{\Delta u}+v\,[u]\,. \tag{3}$$

If Δu is small enough, the incremental quotients can be replaced by derivatives, such that:

$$x_i = -\frac{dv}{du}. \tag{4}$$

The explicit form of the function y_i in terms of x_i is then:

$$y_i = u\,(x_i)\,x_i + v\,[u\,(x_i)]\,, \tag{5}$$

where $u\,(x_i)$ can be found from Eq. (4).

It is recognized in this last expression the Legendre antitransform of the function that represents the straight lines containing the rays that reach the observer eye. In other words, to find the locus of images it is required to find the expression of the curve to which the rays, or their asymptotes, are tangent. Then, different observers see point images of a given point object at different positions, although always on the corresponding caustic curve. This result is valid whenever a small beam of rays entering a detection system is considered.

3. Application to an elementary case

Let us consider a flat horizontal interface between the vacuum and a transparent medium with constant refractive index, n, represented in panel a) of Fig. 1 by the upper half-space and the lower half-space, respectively. For our purpose we choose a Cartesian reference frame whose origin is a point on the interface, with the positive y semi-axis upwards and the positive z semi-axis perpendicular to the drawing plane to the reader. Due to the symmetry of the problem, we can ignore the z coordinate. A ray of light emitted by a point source located at (0,y_s) in the lower half-space ($y_s < 0$) is refracted at the interface. We have called θ_i and θ_t the incidence and transmission angles, respectively.

Let u and v in Eq. (1) be the slope and the y-axis intercept of the line containing the transmitted ray. On the one hand, from Fig. 1 it is apparent that:

$$u = \cot\theta_t, \tag{6}$$

and

$$y_s\tan\theta_i = \frac{v}{u}. \tag{7}$$

On the other hand, from Snell's law the following expression is obtained:

$$n\sin\theta_i = \frac{1}{\sqrt{1+u^2}}. \tag{8}$$

From Eqs. (7) and (8) we finally obtain the following expression:

$$v = \frac{y_s u}{\sqrt{n^2u^2+n^2-1}}, \tag{9}$$

which represents the relation between the slopes and y-axis intercepts of each of the lines containing a refracted ray at the interface. So, Eq. (9) is the Legendre transform of the function we intend to find, and for which Eqs. (4) and (5) are valid. Therefore, using the expression for v given by Eq. (9) in Eq. (4), we get:

$$x_i = \frac{-y_s\left(n^2-1\right)}{\left(n^2u^2+n^2-1\right)^{3/2}}. \tag{10}$$

From the last relation, u can be expressed in terms of x_i as follows:

$$u(x_i) = \frac{1}{n}\sqrt{\left[\frac{-y_s\,(n^2-1)}{x_i}\right]^{2/3}-(n^2-1)}. \tag{11}$$

Substituting this expression in Eq. (9) to get $v[u(x_i)]$, and substituting next x_i, $u(x_i)$ and $v[u(x_i)]$ in Eq. (5), we write the expression for y_i as:

$$y_i = \frac{1}{n}\sqrt{\left[\frac{-y_s\,(n^2-1)}{x_i}\right]^{2/3}-(n^2-1)} \times\left[x_i+\frac{-y_s^{2/3}x_i^{1/3}}{(n^2-1)^{1/3}}\right], \tag{12}$$

which in turn can be written as:

$$y_i = \frac{\sqrt{n^2-1}}{n}\sqrt{\frac{(-y_s)^{2/3}}{(n^2-1)^{1/3}}-x_i^{2/3}} \times\left[\frac{-y_s^{2/3}}{(n^2-1)^{1/3}}+x_i^{2/3}\right]. \tag{13}$$

This expression is the Legendre antitransform of $v\,(u)$, and represents the locus of all the images that could be detected from anywhere in the first quadrant. To give it an even simpler form, we introduce the constant x_l, which represents the abscissa of the point on the surface where the transmitted ray is horizontal. Since the angle of incidence for this position is the so-called limit angle, θ_l, above which total reflection occurs, x_l can be written as:

$$x_l = -y_s\tan\theta_l = \frac{-y_s}{\sqrt{n^2-1}}. \tag{14}$$

Using this new constant, the expression (13) is written as:

$$y_i = \frac{\sqrt{n^2-1}}{n}\sqrt{x_l^{2/3}-x_i^{2/3}}\left[-x_l^{2/3}+x_i^{2/3}\right]. \tag{15}$$

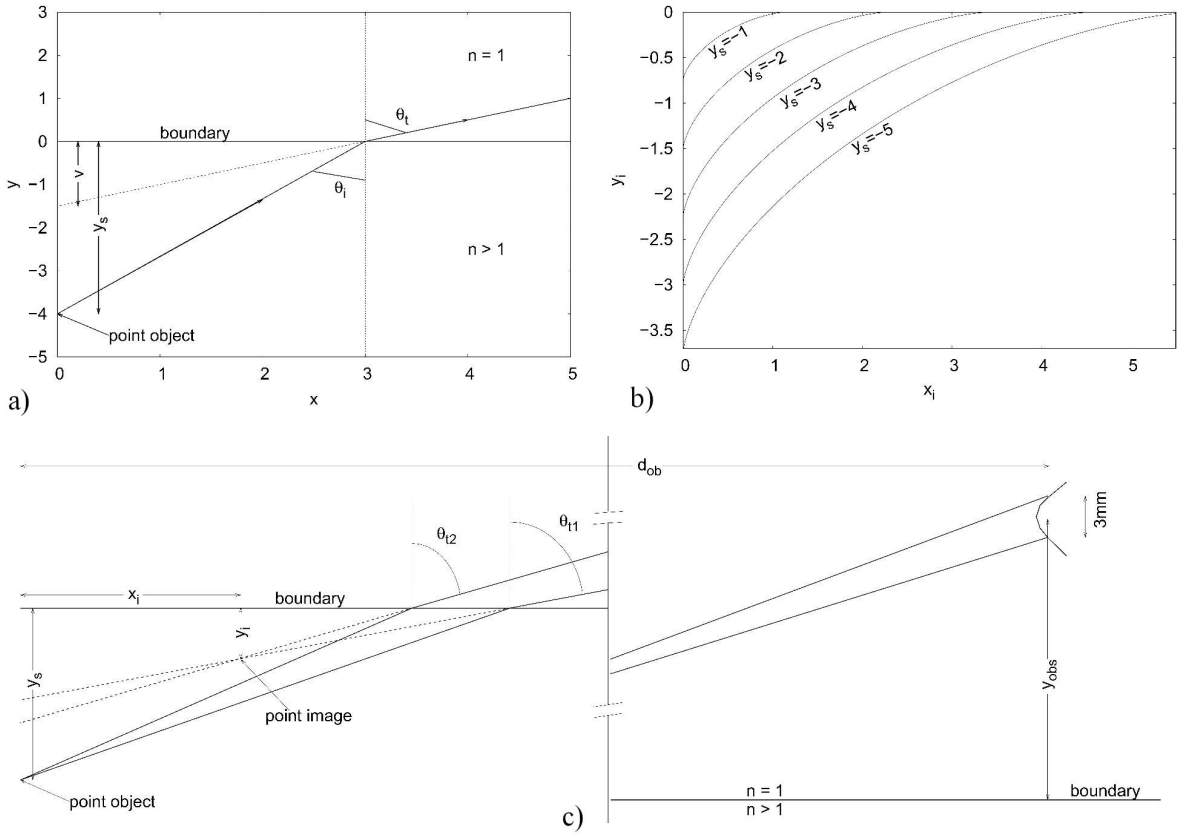

FIGURE 1. Plane-horizontal interface between the vacuum and a transparent medium of refractive index n: image formation. Panel a): trajectory of a light ray emitted by a point object located at $(0, y_s)$. Panel b): curves representing the images positions seen by observers located in different points of the first quadrant, for different y_s values. Panel c): trajectory of light rays emitted by a point object located at $(0, y_s)$ arriving to the observer eyes.

In panel b) of Fig. 1 several curves representing Eq. (15) are shown. With x_i and y_i expressed in the same arbitrary units, each of the curves corresponds to a different y_s value. In order to bear out that Eq. (15) effectively represents the locus of images, we have proceeded as follows: assuming a 3 mm in diameter pupil, we calculate the intersection point of the extensions of the two rays that, at a distance to the object to the observer d_{ob}, pass at $y_1 = y_{ob} + 1.5$ mm and $y_2 = y_{ob} - 1.5$ mm from the ground, where y_{ob} is the height of the observer's eyes. The equations of the lines containing these rays are easily obtained considering that their slopes are $\tan(\theta_{t1})$ and $\tan(\theta_{t2})$, being θ_{t1} and θ_{t2} the transmission angles of the respective rays, and taking into account that, while one of them passes through the point (d_{ob}, y_1), the other passes through the point (d_{ob}, y_2). In order to relate the different parameters, geometric considerations have been made in a scheme that represents the situation, such as the one shown in panel c) of Fig. 1. Next, for each pair of values (d_{ob}, y_{ob}), we have numerically found the pairs of values (x_i, y_i) that satisfy the equations set. The results obtained match those obtained by means of Eq. (15).

All the calculations have been made assuming $n = 1.33$, so the curves shown in panel b) of Fig. 1 would correspond very closely to a water-air interface. Each of the curves in the figure could then represent the locus, in a propagation plane, of the images of a point object located at y_s, for example in a fish tank or a pond, according to the different observer positions looking from above. Given the assumed azimuthal symmetry, these results are valid in each propagation plane. To extend this analysis to every observers located in the upper half-space, it is sufficient to generate a caustic surface of revolution by rotating the curve given by Eq. (15) around the y-axis. All the rays that originate from the point object and reach the observer's eye have been refracted in such a way that their extensions are tangent to the aforementioned caustic surface.

4. Application to inferior mirages

In this section we intend to find the Legendre antitransform of the asymptotics lines to the light rays that reach the observer eyes at the time of an inferior mirage. The expression of this antitransform allows to represent, in each propagation plane, the curve on which the images of a point object are located for different observers.

Adopting a reference frame with the x-axis parallel to the ground and the y-axis perpendicular to it, on theoretical and observational arguments, we have shown in a previous

work [13] that, on the occasion of a inferior mirage, the refraction index varies with the y-coordinate as:

$$n\left(y\right)=n_f\left[1-\alpha\exp\left(-\frac{y}{\beta}\right)\right], \tag{16}$$

where n_f is the n value in the field (*i.e.*, far from the ground), being α and β positive constants for given atmospheric conditions, to be determined in each particular case. We have neglected any small variation of n with x or z, considering all meteorological variables as constants in each plane parallel to the ground.

In the case of a inferior mirage, a ray of light coming from some object, located at a height h, reaches a minimum height y_0, before continuing its upward journey. We called V point that point of closest approach of the ray to the ground. Adopting a coordinate system such that $(0, y_0)$ are the coordinates of V point, and using Eq. (16) for representing n, we have found the following expression [13]:

$$x=2\beta\gamma\ln\left(1+\sqrt{1-\exp\left(-\frac{y-y_0}{\beta}\right)}\right)+\gamma\left(y-y_0\right), \tag{17}$$

to represent the trajectories of light rays on a propagation plane when an inferior mirage occurs, where γ is given by:

$$\gamma=\frac{1-\alpha\exp\left(-\frac{y_0}{\beta}\right)}{\sqrt{2\alpha}\exp\left(-\frac{y_0}{2\beta}\right)}. \tag{18}$$

Since α is of the order of 10^{-5} [13], $\alpha\exp\left(-y_0/\beta\right)\ll 1$, and thus, from Eq. (18), γ can be expressed as:

$$\gamma=\frac{\exp\left(\frac{y_0}{2\beta}\right)}{\sqrt{2\alpha}}. \tag{19}$$

Respect to a coordinate system with $x=0$ at the object position, Eq. (17) becomes:

$$x=2\beta\gamma\ln\left(1+\sqrt{1-\exp\left(-\frac{y-y_0}{\beta}\right)}\right)+\gamma\left(y-y_0\right)+x_v, \tag{20}$$

where x_v is the distance to the object to the V point of the ray, and it can be written as:

$$x_v=2\beta\gamma\ln\left(1+\sqrt{1-\exp\left(-\frac{h-y_0}{\beta}\right)}\right)+\gamma\left(h-y_0\right). \tag{21}$$

As shown in Paola *et al*. [13], the curves representing the light ray trajectories very quickly approach their asymptotes, merging with them a few millimeters beyond V point. Therefore, we consider that each light ray that reaches the observer eyes arrives in the direction of the asymptote to its trajectory, whose equation is:

$$y=\frac{1}{\gamma}x-\beta\ln 4+y_0, -x_v/\gamma, \tag{22}$$

as it was obtained from Eq. (20) taking into account that the exponential tends to 0 for very large y values.

Considering that the light beam entering the pupil is very small, the locus of the images of a point object as the observer position varies can be found in each propagation plane using the result obtained in Sec. 2. We must then find the expression of the curve to which the asymptotes to the rays are tangent or, what is the same, the Legendre antitransform of the function relating y-intercept and slope of the asymptotes to the rays reaching the observer eye. From Eqs. (21) and (22) it follows that:

$$u=1/\gamma, \tag{23}$$

and

$$v=-\beta\ln 4+y_0-x_v/\gamma. \tag{24}$$

Substituting Eq. (19) in Eq. (23) we get:

$$u=\frac{\sqrt{2\alpha}}{\exp\left(\frac{y_0}{2\beta}\right)}, \tag{25}$$

from where we infer the following expression for y_0 as a function of u:

$$y_0=2\beta\ln\left(\frac{\sqrt{2\alpha}}{u}\right). \tag{26}$$

Replacing x_v by Eq. (21) in Eq. (24), and taking into account Eq. (26), we get:

$$v(u)=-\beta\ln 4+2\beta\ln\left(\frac{2\alpha}{u^2}\right)-h-2\beta\ln\left(1+\sqrt{1-\frac{2\alpha}{u^2\exp(h/\beta)}}\right). \tag{27}$$

Taking into account that $(2\alpha/u^2\exp(h/\beta))=(2\alpha\gamma^2/\exp(h/\beta))\ll 1$ we obtain for v:

$$v(u)=2\beta\ln\left(\frac{\alpha}{2u^2}\right)-h. \tag{28}$$

From the last expression we get:

$$x_i=-\frac{dv}{du}=\frac{4\beta}{u}, \tag{29}$$

so that:

$$u(x_i)=\frac{4\beta}{x_i}, \tag{30}$$

and

$$v[u(x_i)] = 2\beta \ln\left(\frac{\alpha x_i^2}{32\beta^2}\right) - h. \tag{31}$$

Substituting then x_i, $u(x_i)$, and $v[u(x_i)]$ in Eq. (5) by the expressions found, we arrive at the following expression for y_i as a function of x_i:

$$y_i = A_1 \ln(x_i) + A_2, \tag{32}$$

where

$$\begin{cases} A_1 = 4\beta \\ \\ A_2 = 4\beta - h + 4\beta ln\left(\frac{\sqrt{\alpha}}{4\beta\sqrt{2}}\right) \end{cases}, \tag{33}$$

where x_i and y_i represent in this case the distance to the object and the height from the ground, respectively, at which the image of a point object is formed, in any vertical plane containing the axis of symmetry of the system. Notice that Eq. (32) is the Legendre antitransform of Eq. (27) and represents the family of curves, one for each value of h, where the images of all point objects are located. That is, whatever the location of the observer (height from the ground and distance to the object), the image of a point object is a point on one of those curves.

5. Results

5.1. Locus of the images in a vertical plane passing through the object

We have searched for the locus of the images (*i.e.*, y_i as a function of x_i) using, on the one hand, Eq. (32). On the other hand, and to confirm our results, we have proceeded in a similar way as we have done in the previous section when considering an elementary case: assuming a 3 mm in diameter pupil and the observer's eyes at y_{ob}, we calculate the intersection point of the asymptotes to the two rays that, at a distance d_{ob} from the object, pass at $y_1 = y_{ob}+1.5$ mm and $y_2 = y_{ob}-1.5$ mm from the ground. To do this, we have first had to numerically find the y_0 values of the two rays that fulfill passing through (d_{ob}, y_1) and (d_{ob}, y_2), respectively. The same results have been achieved by one way or the other. The analysis of the intersection points of the asymptotes to the rays reaching the observer eye allows, additionally, to study, separately, the behavior of x_i and y_i with d_{ob}.

In Fig. 2, for a point object located at $h = 5$ cm from the ground, we represent: in panel a), the horizontal distance to the object, x_i, at which its image is formed as a function of the distance to the observer, d_{ob}. In panel b), the height from the ground, y_i, at which that image is formed, also as a function of d_{ob}. Finally, in panel c), y_i as a function of x_i for each value of d_{ob}. The three panels show results for different values of the height of the observer's eyes. Similar results are shown in the following six panels for point objects located at $h = 50$ cm, in panels d), e), and f), and $h = 200$ cm, in panels g), h), and i). In all the panels, two sets of curves are displayed, drawn with solid lines the ones and with broken lines the others, corresponding to $\alpha = 1.1086 \times 10^{-5}$, $\beta = 0.33$ cm, and $\alpha = 2.2445 \times 10^{-5}$, $\beta = 0.62$ cm, respectively. Whatever the values of these parameters, in Fig. 2 is seen that, on the one hand, as the observer moves away from the object, the position of the image also moves away, although, as the observer-object distance increases some kilometers, the image-object distance increases only a few meters. For given values of α and β, the rate at which x_i changes with d_{ob} depends on the height of the observer's eyes. If $\alpha = 1.1086 \times 10^{-5}$ and $\beta = 0.33$ cm, for example, x_i increases by 14 m as the observer moves 1 km away from an object located 50 cm above the ground, if his/her eyes are 50 cm from the ground, and only about 5 m if his/her eyes are 200 cm from the ground. This behavior is similar for all objects regardless of their height from the ground, although it is less pronounced for higher objects. In other words, the variation of x_i with d_{ob} is less notable both, for higher h and for higher y_{ob}. It is worth pointing out that, for a given observer-object distance, the images of the point objects closest to the ground are formed further from the object, that is, closer to the observer, than those of the highest point objects.

Regarding the dependence on α and β, it can be mentioned that higher values of these parameters imply, in general, higher temperature conditions and greater air temperature gradients near the ground [8]. In Fig. 2 it is observed that the images are formed further from the object for higher values of α and β, being x_i in all the cases some tens of meters long, except for the most extreme weather conditions and point objects very close to the ground. In the latter case, x_i could be a few hundred meters long if the observer's eyes are less than 1 m from the ground. Under these conditions, the nonlinear increase of x_i with d_{ob} observed in panel a) of Fig. 2, unlike what is observed in most cases, is striking. This is a consequence of the behavior of the V points of the rays starting from a given point object. At the beginning, the greater the angle the ray form with the normal to the ground, the greater y_0 (altitude) and the greater x_v (distance to the object), as we have shown in Cruzado *et al.* [8]. However, this behavior extends up to a maximum distance, from which the V points corresponding to y_0 values increasingly closer to h become closer to the object, so that $x_v = 0$ if $y_0 = h$. Although this behavior is the same for all h values, the maximum distance reached by the V points increases very quickly with h, so that it is not apparent for the highest point objects in the range of distances considered in the figure.

On the other hand, in panel b) of Fig. 2 it is observed that the higher the object point is, the lower the height under the ground at which the image is formed, revealing the fact that the image is inverted respect to the object in the case of inferior mirages. As the observer moves away from the object, the height from the ground at which the image of an point object is formed also increases, although not in a linear way as x_i does. The y_i behavior with h, y_{ob}, α and β is similar to that of x_i, although y_i variations, as different parameters

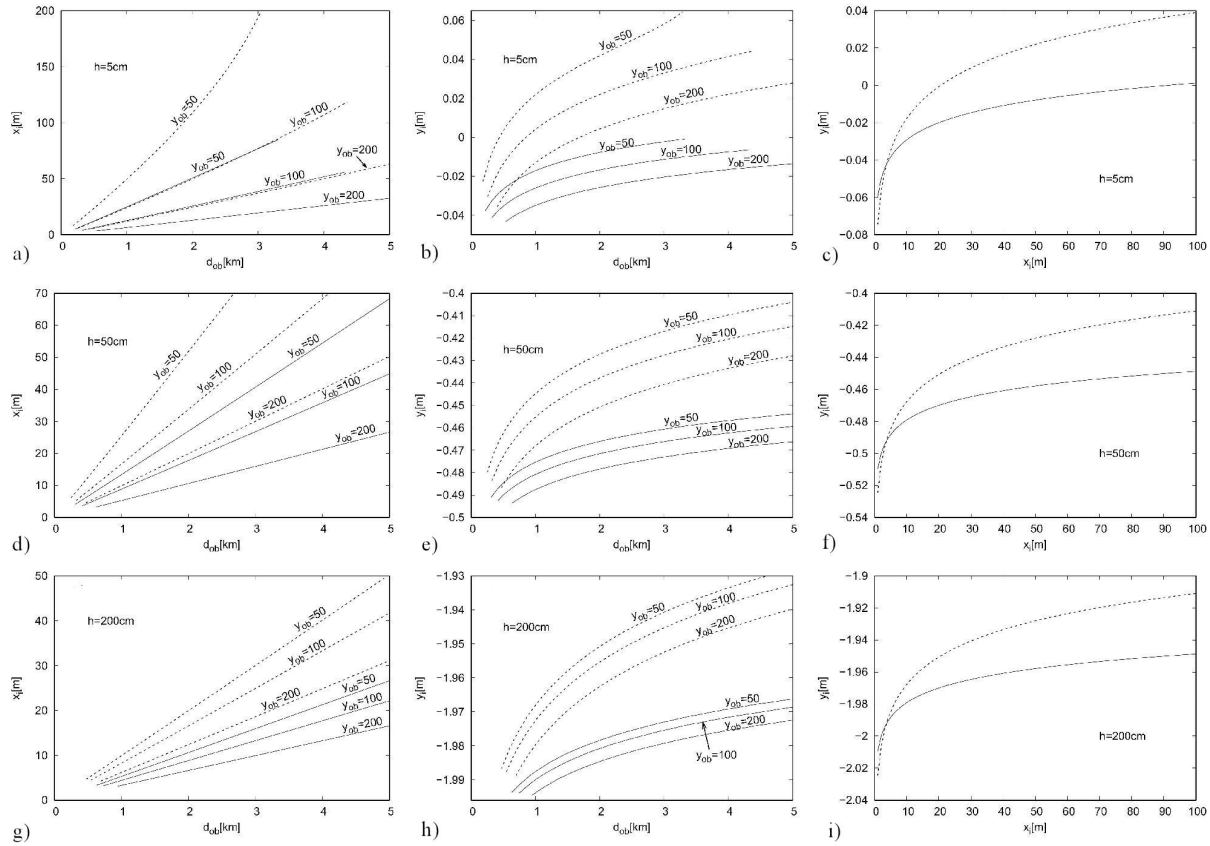

FIGURE 2. Inferior mirage: Location of the images. For a point object at $h = 5$ cm from the ground, panel a) shows the x position of the image, x_i, as a function of the distance to the observer, d_{ob}, panel b) shows the y position of the image, y_i, as a function of the distance to the observer, d_{ob}, and panel c) shows y_i as a function of x_i. Panels d), e) and f): idem panels a), b), and c) for $h = 50$ cm. Panels g), h) and i): idem panels a), b), and c) for $h = 200$ cm.

vary, are only a few millimeters wide. Also revealed here is the behavior of the V points for small h and y_{ob} values and more pronounced vertical temperature profiles. Under these weather conditions, it is also remarkable for small h values that, even though the image of the object is still inverted, y_i, which in the vast majority of cases is below 0, takes positive values. So, sometimes, the image of the base of the objects could be located above the ground if the observer is far enough from the object. For example, for $\alpha = 2.2445 \times 10^{-5}$ and $\beta = 0.62$ cm, the image of every point object located at $h \leq 5$ cm is formed above the ground in every propagation plane, if the observer is more than 850 m from the object and his/her eyes 1 m above the ground.

As a result of the behavior of x_i and y_i with the different parameters that we have just explained, y_i is a smooth increasing function of x_i, as it is displayed in panels c), f), and i) of Fig. 2 for different h values and two different pairs (α, β). Then, given h, α, and β values, the image position of a point object on the corresponding curve depends on the observer position.

For a better understanding of what is expressed in this section, and as a summary, we include Fig. 3, which was achieved assuming $\alpha = 1.1086 \times 10^{-5}$ and $\beta = 0.33$ cm. In this figure we represent with solid lines some of the light rays that, starting from a point object located 5 cm from the ground, are refracted in the lowest atmospheric layers and deflected upward, to occasionally reach the observer's eyes. With dashed lines we represent the asymptotes to the refracted rays, whose envelope forms the corresponding caustic curve. We consider three observers, located all of them 120 m

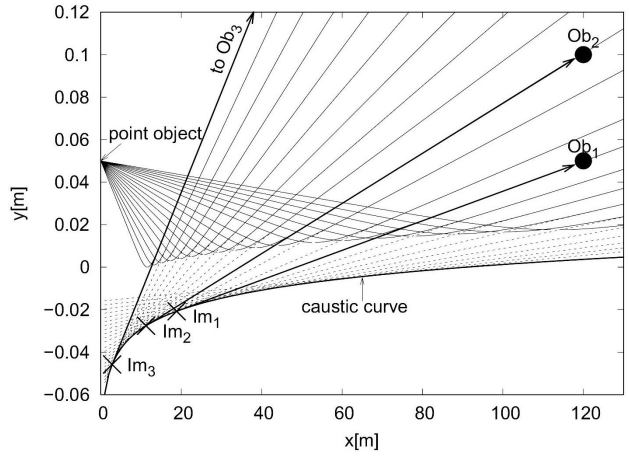

FIGURE 3. Point object and its images, Im_1, Im_2, and Im_3, on the caustic curve, for three different observers, Ob_1, Ob_2, the third being out of the graph (see text for explanation).

from the object, with their eyes at three different heights from the ground, namely, $y_{ob} = 5$ cm, $y_{ob} = 10$ cm, and $y_{ob} = 50$ cm. Two of the observers are represented with filled circles in the figure, and the direction to the third, who is out of the graph, is indicated. With crosses we represent the different positions of the image of the point object, as they would be seen by each of the three observers. With thick solid lines we highlight the ray (and its asymptote) that, in each case, reaches the observer's eyes and forms the corresponding image.

5.2. Locus of the images in the space

We remind the reader that, as we explained at the beginning of Sec. 2, we have analized what happens in each propagation plane. Therefore, the images of point objects would be located on the curves shown in panels c), f), and i) of Fig. 2 if the light beam arriving at the detector had a negligible horizontal opening, as it would happen, for example, if the detector were a vertical slot. In addition, we are interested on analyzing where a human observer would see the images of a point object at the time of an inferior mirage, taking into account that a beam of light with both, vertical and horizontal aperture, contributes to the formation of images at the retina, and also that a casual observer likely view the phenomenon with both eyes. We are not interested in ocular aberrations and assume a perfectly circular, normal pupil.

To begin the analysis, let us first take a closer look at what happens in each propagation plane, by considering the asymptotic lines to the rays that, starting from a point object, reach the upper and lower edge of a human pupil. The extensions of these straight lines, after intersecting each other at the point (x_i, y_i) on the corresponding caustic surface, as we have just seen, intercept the y-axis, on which the object is located, at two points that are nothing but the y-intercept of the respective lines. The situation is represented in Fig. 4 panel a), where O_1 and O_2 are the mentioned y-intercepts. Given the minimum distances to the object, d_{min}, at which an observer should be located to view the mirage, as it was analyzed in Cruzado *et al*. [8], and considering the values of $x_i \ll d_{\min}$ found in the present work, it is prompt to infer that O_1 and O_2 are very close to each other. To see the image of a vertically extended object from its base, for example, an observer with his/her eyes at $y_{ob} = 1.8$ m from the ground should be at least 386 m away from the object, if $\alpha = 1.1086 \times 10^{-5}$ and $\beta = 0.33$ cm, while x_i is only a couple of tens meters long, as seen in Fig. 2. In fact, we have been able to calculate that O_1 is always only a few hundredths of a millimeter from O_2. In a scale graph the points O_1 and O_2 would not be distinguishable from each other.

Given the azimuthal symmetry assumed for the problem, the situation described corresponds to any vertical plane containing the y-axis, as it is represented in Fig. 4 panel a). It could be said then that all the rays that start from a point object and reach the detector intersect each other at a point on the y-axis.

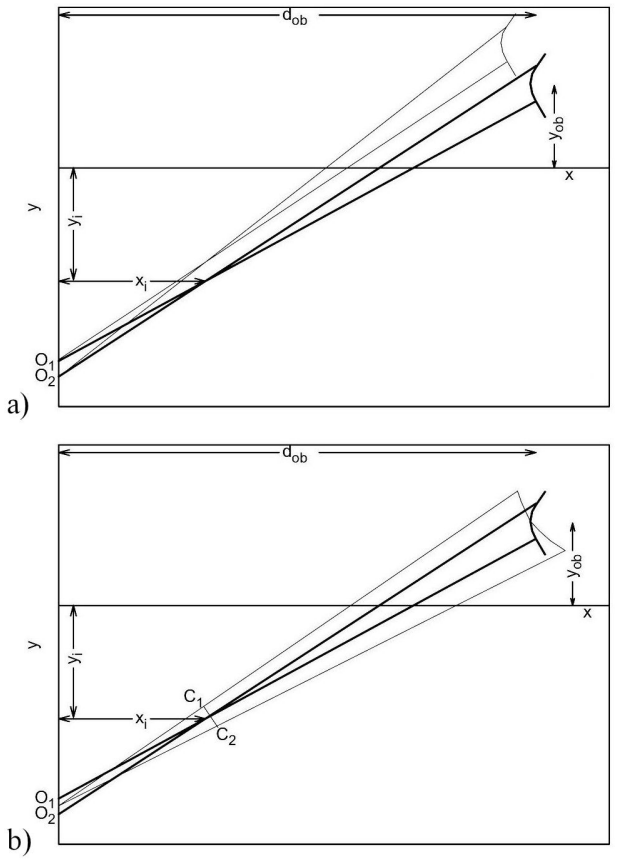

FIGURE 4. Panel a): asymptotic lines to the rays arriving to the upper and lower edges of a human pupil, in two different propagation planes (see text). Panel b): asymptotic lines to the rays arriving to the upper and lower edges, in a propagation plane, and to the lateral edges of a human pupil (see text).

To take into account the horizontal opening of the light beam, let us consider the asymptotes to the two rays that, starting from a point object, reach the lateral edges of a human pupil. Each of these extreme lateral rays is contained in their own propagation plane, so neither they nor their asymptotes intersect each other anywhere between the point object and the eye. However, each of these rays is tangent to the caustic surface at the point where the rays reaching the upper and lower borders of the pupil, in the corresponding propagation plane, intersect. These extreme lateral rays draw a small horizontal segment on the caustic, as represented by C_1C_2 in Fig. 4 panel b), and intersect each other at a point midway between O_1 and O_2 on the y-axis. It should be noted that the small horizontal segment C_1C_2 on the caustic is as large as the vertical segment O_1O_2 on the y-axis. In a real situation, no naked eye observer could distinguish C_1 from C_2, nor O_1 from O_2. This can be verified by comparing the angular size of the portion of the caustic C_1C_2 subtended at the eye, ϕ hereafter, with the resolving power of the human eye, as Berry [3] did. Using the Rayleigh criterion to express the minimum angle ϵ that the eye can resolve, and expressing ϕ in terms of the distance to the observer and the radius of curvature of the caustic, Berry [3] arrived to the expression

$$\frac{\phi}{\epsilon} = \frac{R}{2.44\lambda}\left(\frac{a}{d'_{ob}}\right)^3, \tag{34}$$

where R stands for the radius of curvature of the caustic, d'_{ob} the distance from the observer to the image (on the caustic), a the human pupil diameter, and λ the wavelength of the light. According to Berry [3], caustics are observable provided the ratio ϕ/ϵ exceeds unity. Taking into account the small values of x_i calculated in the previous section, it is clear that $d'_{ob} \approx d_{ob}$. R can be calculated as a function of x from Eq. (32), being apparent from Fig. 2 and 3 that R increases with x. Adopting $\lambda = 5000$ Å, we have verified that the ratio ϕ/ϵ increases as d_{ob} decreases and exceeds unity for d_{ob} values less than the minimum distances at which the observer should be located to witness a mirage. In the most extreme case, and very unlikely one, if the observer's eyes were 1 cm from the ground, to see the image of the object points closest to the ground the observer would have to be at least 6 m from the object, while ϕ/ϵ becomes equal to 1 at $d_{ob} = 5$ m.

Anywhere between the object and the observer, the rays entering the pupil draw an ellipse in a plane perpendicular to them. Near the observer it is a horizontal major axis ellipse that flattens out as the distance to the observer increases, becoming the segment C_1C_2 on the caustic. From there, the ellipse is deformed in such a way that it turns to a vertical major axis ellipse, eventually becoming the segment O_1O_2 on the y-axis. Between the segments C_1C_2 and O_1O_2 the rays shape a circle called the circle of least confusion. The reader likely recognizes in this description the situation that an astigmatic eye generates. Astigmatism is a refractive error caused by an irregularity in the shape of the eye, resulting in blurred vision. However, we have assumed a perfectly circular normal pupil and the described astigmatism is introduced in this case by the atmosphere, which is found in the particular conditions that would give rise to inferior mirages. Although the segments C_1C_2 and O_1O_2 are very short, they are not theoretically points. Then, in looking at with only one eye, the observer would see the image where the circle of least confusion is located, if the resolving power of the eye allowed it. Instead, taking into account that the eyes are about 6 cm apart, if an observer were to look at the phenomenon with both eyes, the horizontal opening of the beam would be much greater than the vertical one, and the observer sees the image on the y-axis passing through the object. Then, assuming that casual observers look at the phenomenon with both eyes, the image coordinates are $x = 0$ and $y \approx O_1 \approx O_2$ respect to a reference frame such that the object is on the y-axis.

To illustrate these results and as an example we have included the Figs. 5, 6, 7, and 8. In Fig. 5, adopting a coordinate system (x,y,z) such that the plane (x,z) is on the ground and the y-axis is perpendicular to it, an object 0.5 m tall and 2 m wide, which might be a bush, is shown. The object is located with its axis of symmetry perpendicular to the ground, 500 m from an observer and with one of its faces, the one represented with the thick line in Fig. 5, oriented towards him/her. We assume that the face of the object in front of the observer, who is looking from (0,1.8,0) in the figure, is the only one from which light rays can reach him/her. Let us consider as object 1 the face oriented to the observer of the object represented in Fig. 5.

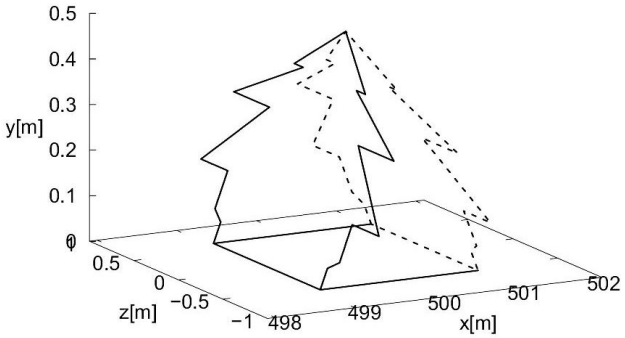

FIGURE 5. Object located with its axis of symmetry perpendicular to the ground, 500 m from an observer whose eyes are located at (0,1.8,0). The face of the object represented by a thick line is facing the observer, while the opposite face, represented by a dashed line, is invisible to him/her.

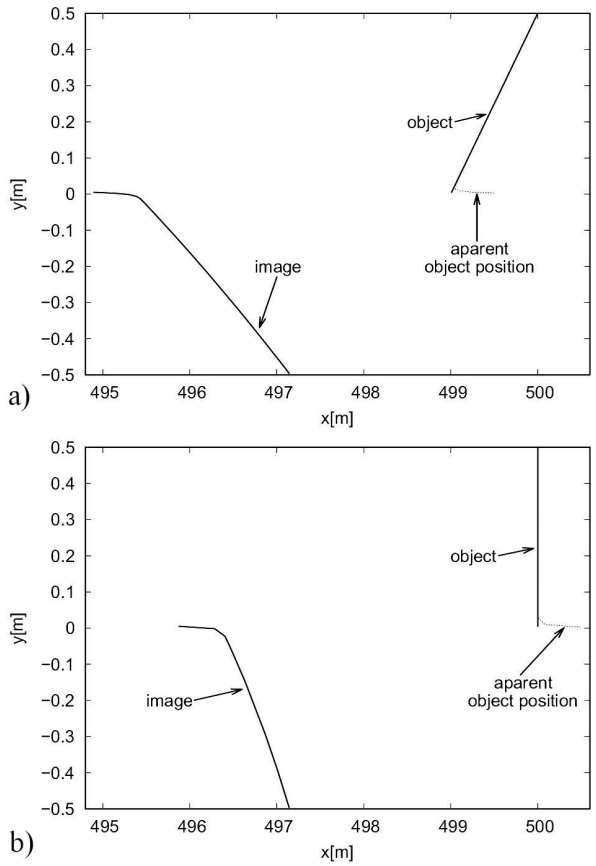

FIGURE 6. Object position, image position, and apparent object position (see text) in a propagation plane. Panel a): the positions of object 1 and its inverted image are displayed with solid lines and the apparent position of object 1 is displayed with dashed lines. Panel b): idem panel a) for object 2.

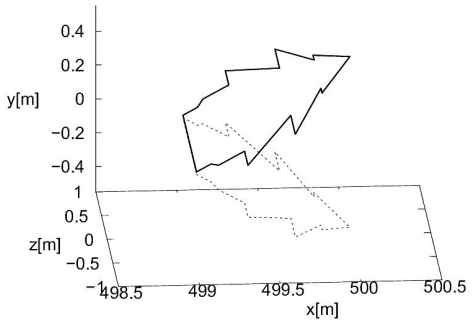

FIGURE 7. Object 1 and its image in the position in which an observer would see them looking at the phenomenon with both eyes located at (0,1.8,0).

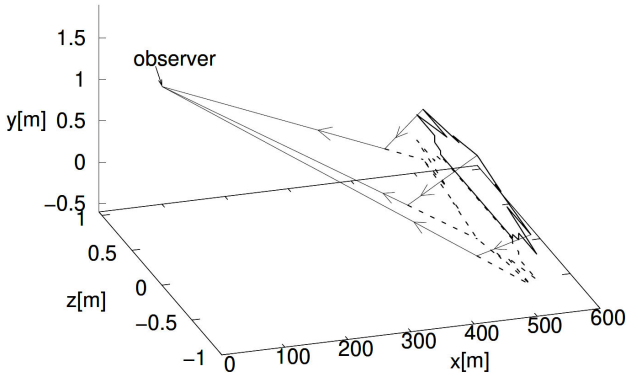

FIGURE 8. Idem Fig. 7 but including the observer, located 500 m from the object. Some rays starting from different points on the object and reaching the observer's eyes are represented with arrows. The asymptotes to those rays are represented with dashed lines.

In panel a) of Fig. 6 the positions of this object and its inverted image are displayed with thick solid lines as they would be formed in each propagation plane. We can clearly confirm the conclusions reached in Sec. 5.1. In particular, it is observed that the images of the points of object 1 very close to the ground are formed visibly closer to the observer than the others, not being this due only to the fact that the lower part of object 1 is closer to the observer than its upper part, as we show below. The dashed line in Fig. 6 represents the apparent position of object 1, that is, the position in which it would appear to be located once the light has passed through a device as a vertical slot located at 1.8 m above the ground. To understand the meaning of this, it must be taken into account that the rays that, starting from any point object, go directly upwards and eventually reach a detector, also deviate from their original rectilinear path due to atmospheric refraction. Therefore, the position of an object as detected by the slot or seen by the observer in a vertical plane does not exactly match its actual position. This effect is more pronounce as the point object is closer to the ground, where the vertical gradient of temperature, and therefore of n, is greater. To represent it in Fig. 6, Eq. (20) and Eq. (22) have been used again to represent the trajectories of the rays and their asymptotes, but keeping in mind that $x_v \leq 0$ for the rays arriving directly from the object to the detector. Since the analysis of the apparent position of the object involves the same equations as those used to analyze the position of the image, similar conclusions are inferred. The apparent difference in Fig. 6 is that, the points of the object closest to the ground imply apparent positions located further away from the observer. In panel b) the curves have the same meaning as in panel a), although they correspond to another object, named object 2. This new object is similar to the previous one but, unlike object 1, it is located vertically to the ground. It is evident that, even in this case, the images of the points very close to the ground are formed closer to the observer than the others, even though the lower and upper parts of object 2 are at the same horizontal distance to the observer.

In Ref. [7], the object 1 and its image, in the position in which an observer would see them looking at the phenomenon with both eyes, are displayed. From what has been said in previous paragraphs, it is clear that the image of each point belonging to the object is formed at a distance to the observer equal to the distance at which this point is located. As for the height from the ground where the images are formed, they are given by the y-axis intercept of any of the asymptote to the rays that, starting from the considered point, enter the eyes of the observer. In Fig. 8 we have also included the observer, located 500 m from the object, some rays starting from different points on the object and reaching the observer's eyes at 1.8 m above the ground, and the asymptotes to those rays which form the corresponding images. It is clearly seen from Fig. 8 that, at such a great distance from the object, the observer will not distinguish the differences in distances to different points on the object, nor to different points on the image. As a consequence of the limited depth perception of our eyes beyond a a few meters, the observer will see the entire object and the entire image on the same plane.

Regarding changes of image topology, it can be analyzed within the framework of the caustic touching theorem introduced by Berry [4]. Berry's theorem was applied, for example, to reflection in mirrors whose curvature changes sign by Berry himself in Ref. [5] and to reflection in plane and spherical mirrors by Silva-Ortigoza *et al*. in Ref. [15]. According to this theorem, topological changes appear when the object touches the "caustic of the family of imaginary rays emitted by the observing eye". It should be noted that in the case of inferior mirages the caustics are virtual and they are, in most cases, below the ground. The caustic curves of imaginary rays emitted by the observing eye only rise above the ground for positions of the observer's eyes very close to it. As an example, we show in Fig. 9 two caustic curves corresponding to observer's eyes at 8 cm and 10 cm above the ground, for $\alpha = 1.1086 \times 10^{-5}$ and $\beta = 0.33$ cm. It is seen that the caustic curves rise above the ground at distances of 884 and 4022 m, respectively, under the climatic conditions we have

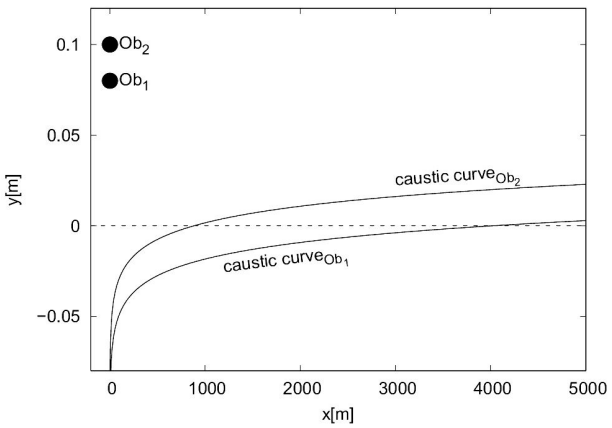

FIGURE 9. Caustic curves of the family of imaginary rays emitted by the observing eye (see text for explanation) corresponding to observing eyes located at 8 and 10 cm from the ground. The ground level is represented with a dashed line.

been adopted. This means that, if the object is at a greater distance to the observer than these values, at least the base of the objects would touch the corresponding caustics. It is clear that this would be a very unlikely situation, so we do not expect casual observers of inferior mirages to witness topological changes in the images of extended objects. However, the topic would deserve a separate, more extensive study, in order to contemplate these and other extreme situations, particularly when very steep temperature gradients occur in the air layers closest to the ground.

6. Summary and conclusions

In this work it was first shown that:

1. as long as the beam of rays entering a detection system, which could be the human eye, has a small aperture, the image of a point object formed by that system in a vertical plane passing through the object is a point, regardless of whether the image formed by a optical system previously traversed by the beam has generated a non-point image of the object;

2. the different images formed by the detection system as its position relative to the object varies, are located on the caustic curve corresponding to the previously traversed optical system.

Then, we have applied these results to two particular cases: i) given a horizontal separation surface between two media of different refractive index, to the images of a point object located in one of the media detected by an observer located in the other, and ii) to the images detected by an observer on the occasion of an inferior mirage. The analytical expressions of the caustic curves (*i.e.*, y_i in terms of x_i), in both cases, have been found by means of the Legendre antitransform of the lines containing the refracted rays, or their asymptotes.

To confirm our results, we proceeded, in both cases, as follows: assuming a vertical aperture of the detection system of 3 mm (equal to a human pupil diameter) and a height from the ground y_{ob}, we calculate the intersection point of the asymptotes to the two rays that, starting from a point object, pass through (d_{ob}, y_1) and (d_{ob}, y_2), respectively, being $y_1 = y_{ob}+1.5$ mm, $y_2 = y_{ob}-1.5$ mm, and d_{ob} the observer-detector distance. This procedure has also made it possible to obtain relevant information on the behavior of y_i and x_i, separately, with parameters such as d_{ob}, y_{ob}, and h, in the case of inferior mirages, a phenomenon of priority interest in this work.

We have also analyzed the influence of atmospheric conditions on this phenomenon by varying α and β values, parameters used to characterize the atmosphere state near the ground. As it was already concluded in previous works, higher temperature values and steeper gradients affect the appearance of the phenomenon in an evident way close to the ground. Finally, and since all the previous analysis refer to what happens in each each of the planes that we have named propagation planes, we have analyzed the appearance of the phenomenon for a real human observer, that is, in space rather than in a plane.

To carry out all the calculations, we have adopted d_{ob} and y_{ob} values such that the observer (or any detector) is able to see the mirage. As this regards, we recall the results achieved in Cruzado *et al*. [8] concerning the regions in each propagation plane where an observer should be located to observe the phenomena. As we show in this previous work, the limits of those regions depend on the atmospheric conditions, which we have been able to include through α and β parameters. Assuming that the refractive index near the ground grows exponentially, as suggested by theoretical arguments and experimental measurements, a proper treatment of the heat transport mechanisms that would take place at the time of a inferior mirage has led us to build a simple model to describe the atmosphere state. This allows to express α and β parameters in terms of three measurable temperature values, which correspond to three different altitudes, namely: ground level, 1 cm, and that at which field temperature is reached. The results shown in this work have been obtained by adopting α and β values that account for feasible temperature profiles in nature. It is important to highlight that the treatment we have carried out allows the reverse path: given the characteristics that the phenomenon shows at the time of its visualization, to infer the atmospheric conditions that are taking place.

1. C. Bellver-Cebreros, M. Rodriguez-Danta, Caustics and the Legendre transform, *Optics Communications* **92** (1992) 187, https://doi.org/10.1016/0030-4018(92)90619-3.
2. C. Bellver-Cebreros, E Gomez-Gonzalez, and M. Rodriguez-Danta, Obtention of meridian caustics and catacaustics by means of stigmatic approximating surfaces, *Pure Appl. Opt.* **3** (1994) 7, https://doi.org/10.1088/0963-9659/3/1/002.
3. M. V. Berry, Reflections on a Christmas-tree bauble, *Phys. Educ.* **7** (1972) 1, https://doi.org/10.1088/0031-9120/7/1/301.
4. M. V. Berry, Inflection reflection: images in mirrors whose curvature changes sign, *Eur. J. Phys.* **42** (2021) 065301, https://doi.org/10.1088/1361-6404/ac1abe.
5. M. V. Berry, Inflection reflection: images in mirrors whose curvature changes sign, *Eur. J. Phys.* **42** 065301 (2021), DOI 10.1088/1361-6404/ac1abe.
6. P. Carpena and A. V. Coronado, On the focal point of a lens: beyond the paraxial approximation, *European Journal of Physics* **27** (2006) 231, https://doi.org/10.1088/0143-0807/27/2/006.
7. A. Cordero-Dávila and J. Castro-Ramos, Exact calculation of the circle of least confusion of a rotationally symmetric mirror, *Applied Optics* **37** (1998) 6774, https://doi.org/10.1364/AO.37.006774.
8. A. Cruzado, A. Cesanelli and C. A. Paola, Light refraction in the earth's atmosphere II. Inferior mirages: regions for images and objects observation, *Rev. Mex. Fís.* **69** (2023) 061303 1, https://doi.org/10.31349/RevMexFis.69.061303.
9. G. Da Costa and R. Escalona, Time evolution of the caustics of a laser heated liquid film, *Applied Optics* **29** (1990) 1023, https://doi.org/10.1364/AO.29.001023.
10. A. V. Gitin, Legendre transformation: Connection between transverse aberration of an optical system and its caustic, *Optics Communications* **281** (2008) 3062, https://doi.org/10.1016/j.optcom.2008.02.003.
11. V. L. Korneĭchik, Connection between the types of residual aberrations and the caustics in the image plane of a lens element, *Journal of Optical Technology* **67** (2000) 995.
12. J. A. Lock and J. R. Woodruff, An analysis of two unusual reflection caustics, *American Journal of Physics* **57** (1989) 260, https://doi.org/10.1119/1.16049.
13. C. A. Paola, A. Cruzado, and F. M. Carrasco Galleguillos, Light refraction in the earth's atmosphere I. Inferior mirages: analytic solution of ray paths, *Rev. Mex. Fís.* **68** (2022) 041301 1-8, https://doi.org/10.31349/RevMexFis.68.041301.
14. G. Silva-Ortigoza, M. Marciano-Melchor, O. Carvente-Muñoz, and R. Silva-Ortigoza, Exact computation of the caustic associated with the evolution of an aberrated wavefront, *Journal of Optics A: Pure and Applied Optics* **4** (2002) 358, https://doi.org/10.1088/1464-4258/4/3/325.
15. G. Silva-Ortigoza, I. Julián-Macías, A. González-Juárez, E. Espíndola-Ramos, R. Silva-Ortigoza, and M. Marciano-Melchor, Exact mirror equation via Berry's caustic touching theorem: plane and spherical mirrors, *J. Opt. Soc. Am. A* **39** (2022) 726, https://doi.org/10.1364/JOSAA.452843.